

Hearing What You Cannot See and Visualizing What You Hear: Interpreting Quartz Crystal Microbalance Data from Solvated Interfaces

Over the last 2 decades, the quartz crystal microbalance (QCM or QCM-D) has emerged as a versatile tool for investigating soft and solvated interfaces between solid surfaces and bulk liquids because it can provide a wealth of information about key structural and functional parameters of these interfaces. In this Feature, we offer QCM users a set of guidelines for interpretation and quantitative analysis of QCM data based on a synthesis of well-established concepts rooted in rheological research of the last century and of new results obtained in the last several years.

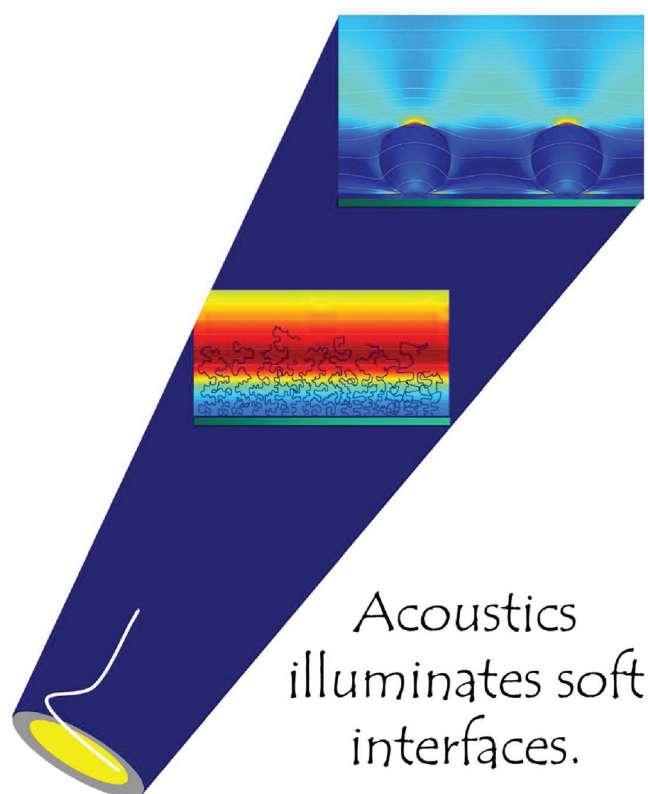
Ilya Reviakine,^{*,†,‡} Diethelm Johannsmann,[§] and Ralf P. Richter^{*,†,||}

[†]Biosurfaces Unit, CIC biomaGUNE, Paseo Miramon 182, 20009 Donostia—San Sebastian, Spain

[‡]Department of Biochemistry and Molecular Biology, University of the Basque Country, 48940 Leioa, Spain

[§]Institute of Physical Chemistry, Clausthal University of Technology, 38678 Clausthal-Zellerfeld, Germany

^{||}Max-Planck-Institute for Intelligent Systems, Heisenbergstrasse 3, 70569 Stuttgart, Germany



The dynamics of soft, solvated interfaces between solid surfaces and bulk liquids is extremely important in fundamental research and technology. Examples of such interfaces include biointerfaces that arise when biological systems interact with inorganic materials: in implants, biosensors, and in purification,

food processing, and marine technologies.^{1–3} They also arise in the case of functional polymer coatings that control the binding or release of molecules of interest and provide lubrication or stabilization.⁴ Their organization is often determined by the interactions with the solvent, making them challenging to investigate and calling for methods that can do so with as little modification (drying, staining) as possible and that can zoom in on the role of solvent in these systems. They are also dynamic: their organization changes in response to external stimuli, chemical or physical, calling for methods that can monitor these changes in real time. Finally, these methods need to be quantitative.¹

Quartz crystal microbalance (QCM or QCM-D)^{5–9} is an instrument that has become widely popular for studying soft and solvated interfaces^{7,10–33} because it is able to meet these challenges. It works in liquids, can monitor changes in the interface organization in situ, with a reasonable time resolution, without requiring labels,^{10,11,14,21,28} and provide information about the solvent inside interfacial films.^{10,17,18,20,22,26,28,34–36} A wealth of information can be extracted from QCM data, and the focus of this Feature is on its quantitative interpretation for thin interfacial films. It is prompted by the recent developments in this area that represent a paradigm shift in the way of interpreting QCM data in terms of the details of the distribution of material at an interface, its coupling to the surface, and the role played by the liquid in which the interfacial layer is immersed.^{28,35–38} Our aim is to formulate guidelines for approaching QCM data interpretation for various experimentally relevant scenarios, arming users with the most recent information about available analysis tools and their principles. Before delving into the topic, we briefly summarize the principles of QCM and its history, highlighting its significant role in soft- and biointerface sciences.

Published: September 22, 2011

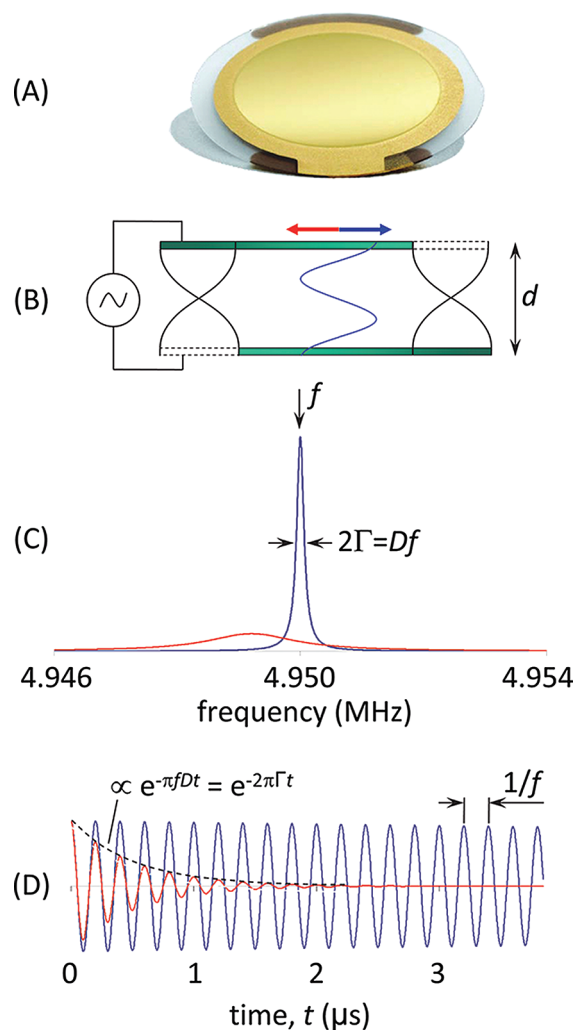


Figure 1. Schematics of QCM and QCM-D operation. (A) A photograph of a 4.95 MHz AT-cut quartz crystal (Q-Sense). The yellow color is due to the gold electrode. (B) Side view of the crystal. Application of oscillatory voltage results in a cyclical deformation, where top and bottom surfaces move tangentially in an antiparallel fashion. The fundamental frequency (black waves at the edges of the crystal) and the third overtone (blue wave in the middle) are illustrated. The motion of the crystal is greatly exaggerated for clarity. In reality, the thickness of the crystal is $\sim 300 \mu\text{m}$, while the amplitude of motion is of the order of at most a couple of nanometers in aqueous solution (it depends on the driving voltage and overtone order).⁸ (C) Resonances observed when a crystal is in air (blue) or in liquid (red). These are the typical spectra obtained with impedance analysis. The excitation frequency (here exemplified by the fundamental frequency) is plotted on the x -axis. The y -axis represents the amplitude of the current passing through the crystal, or equivalently, the amplitude of the crystal's shear motion. Two parameters are used to characterize the resonance: its frequency f and its bandwidth Γ . (D) QCM-D uses a so-called ring-down method, where the driving voltage is intermittently switched off and the decay in time of the oscillation is monitored. From the decay curve, the resonance frequency f and the energy dissipation $D = 2\Gamma/f$ are extracted. The blue decay curve in this figure corresponds to a crystal oscillating in air. The red curve corresponds to the dissipation of 1.6×10^{-1} , a great exaggeration for illustrative purposes. For comparison, the dissipation of a bare crystal in water is $\sim 3.5 \times 10^{-4}$ at the fundamental. The two types of measurements, impedance analysis and ring-down, are strictly equivalent; the two types of curves shown in parts C and D are related to each other by a Fourier transform.

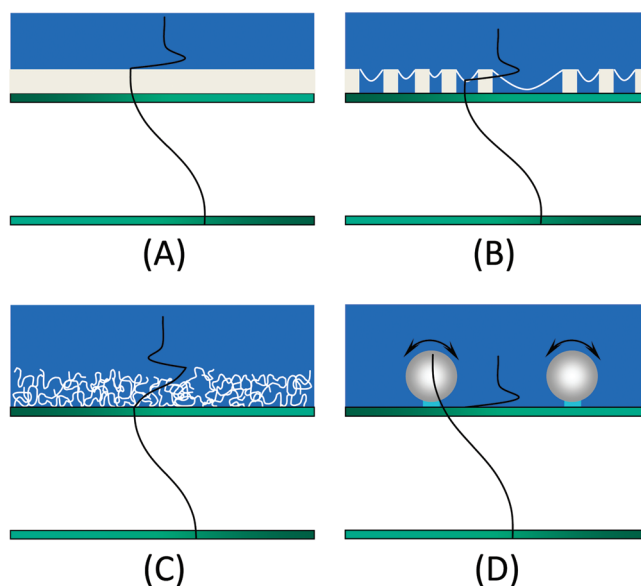


Figure 2. Types of films encountered in QCM experiments. Depositing a film on the surface of a QCM crystal effectively increases the crystal thickness and therefore the wavelength of the standing wave, as shown schematically in this figure. This decreases the resonance frequency. The relationship between film properties and the frequency shift, $\Delta f_n = f_n(\text{bare crystal in bulk liquid}) - f_n(\text{crystal with film in bulk liquid})$, depends on the type of the film. We consider four types of films (Table 1). Films that do not appreciably dissipate energy are shown in parts A and B and films that do dissipate energy in parts C and D. Parts A and C deal with films that can be treated as laterally homogeneous and parts B and D with films that are composed of discrete particles. In all cases, the materials deposited on the crystal are shown in light gray. (A) Thin and homogeneous rigid films: In these films, Δf is proportional to the areal mass density of the film (layer density $\rho_f \times$ layer thickness h_f), eq 1.⁴⁵ (B) Laterally heterogeneous films: Films consisting of discrete particles (adsorbed proteins,^{36,38} virus particles,^{26,37} or detergent micelles²²) that dissipate little energy can also be dealt with by the Sauerbrey relationship,⁴⁵ but in this case the areal mass density contains a coverage-dependent solvent contribution illustrated schematically with curved white lines. (C, D) Dissipating films: In the case of laterally homogeneous films depicted in part C, the dissipation occurs inside the film and is related to the viscoelastic properties of the material through the continuum model (eq 5). In the case of laterally heterogeneous films composed of discrete particles shown in part D, most of the dissipation occurs at the liquid–particle boundary and is related to the properties of the particle–surface contact region (also called “linker”) shown in turquoise underneath the particles.³⁷

WHAT IS QCM

QCM is based on the inverse piezoelectric effect discovered by the Curies in the late 19th century: application of voltage results in mechanical deformation of the material, for crystalline materials with certain symmetry properties.^{5,39} Alternating applied voltage leads to a cyclical deformation, resulting in an oscillatory motion. If the frequency of the applied voltage matches the crystal's resonance frequency (or multiples thereof called overtones), a standing wave is generated inside the crystal. This was realized by Cady,³⁹ who applied it to the construction of stable oscillator circuits.

Depending on the cut of the crystal relative to its crystallographic axes, different kinds of oscillations may arise.^{39–41} AT-cut crystals, used in QCM (Figure 1A), vibrate in the so-called thickness-shear mode, where the two surfaces move in an antiparallel fashion

(Figure 1B). In resonance, crystal surfaces are located at the antinodes of a standing wave with the wavelength $2d/n$, where d is the crystal thickness and n is the overtone order (odd), leading to the resonance frequency $f_n = nc/2d$, where c is the speed of sound in quartz. In liquids and gases, shear-waves decay rapidly, making QCM interface-specific.

There are several ways to perform QCM measurements. One can examine the polarization at the crystal surface as a function of the frequency of the applied voltage, the so-called impedance analysis.⁴² This yields two parameters per overtone, the resonance frequency f_n and the bandwidth Γ_n (Figure 1C). The alternative is the “ring-down” scheme developed by Rodal et al., referred to as QCM-D,⁹ where the external driving voltage is turned off intermittently and the oscillations are left to decay freely. Given that quartz is piezoelectric, a voltage is generated during these decaying mechanical oscillations. This signal is recorded, also yielding two parameters per overtone, the resonance frequency f_n and the dissipation D_n (Figure 1D). Bandwidth and dissipation are equivalent, with $D_n = 2\Gamma_n/f_n$ (Figure 1C,D). We will use both terms interchangeably. The third way to perform QCM measurements is with oscillator circuits. These can be very economic but usually operate on one harmonic only and provide only indirect access to the bandwidth via the oscillation amplitude. This limits the data interpretation severely. All of these approaches require that the quartz crystal is coated with electrodes (typically gold, Figure 1A). Cady³⁹ also describes an electrodeless approach, which has recently been applied to exciting high-frequency crystals particularly sensitive to electrode effects.^{43,44}

The ubiquitous application of quartz crystals in oscillator circuits is based on their exceptional stability and very low energy dissipation. Their use as microbalances is based on the linear relationship between changes in the resonator mass and in the resonance frequency, derived by Sauerbrey (Figure 2A):⁴⁵

$$\Delta f_n = -\frac{n}{C}m_f = -\frac{n}{C}\rho_f h_f \quad (1)$$

where m_f is the areal mass density of the adsorbed film (mass per unit area), and ρ_f and h_f are the density and the thickness of the adsorbed film. The mass sensitivity constant C depends solely on the fundamental resonance frequency f_F and the material properties of the quartz crystal. For crystals with $f_F = 5$ MHz, it is $18 \text{ ng cm}^{-2} \text{ Hz}^{-1}$.

In liquids, first measurements of viscosity with torsional- and shear-quartz resonators date back to the late 1940s.^{40,46} They are based on the relationship between the resonance frequency/bandwidth of a crystal and the liquid's viscosity η_l and density ρ_l :^{46–50}

$$\Delta f_n = -\Delta\Gamma_n = -\frac{f_n}{2}\Delta D_n = -\frac{1}{C}\sqrt{\frac{n\rho_l\eta_l}{2\omega_F}} \quad (2)$$

where $\omega_F = 2\pi f_F$ is the angular fundamental resonance frequency. Equation 2 is typically attributed to Kanazawa and Gordon,⁴⁸ but it appears in a number of earlier publications.^{46,47,49,50} It states that the decrease in the frequency and the increase in the dissipation are both proportional to the square root of the product of liquid viscosity and density. Since QCM is sensitive to the properties of the bulk liquid, a reference measurement in the same liquid is always necessary for separating bulk liquid contribution from the film properties.

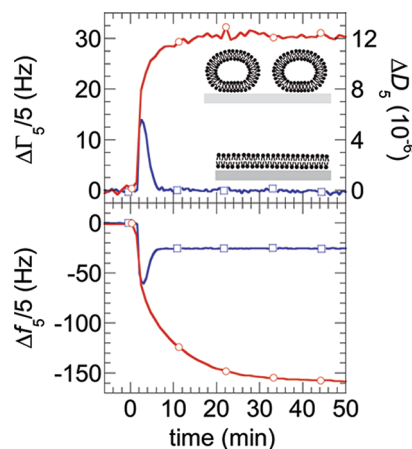


Figure 3. Sensitivity of QCM to layer morphology is illustrated by the archetypical example of liposomes adsorbing on an inorganic surface. Liposomes are quasi-spherical lipid structures developed as cell membrane models. Red curves represent adsorption of intact liposomes to a surface. Blue curves correspond to a scenario where liposomes adsorb initially intact and later rupture into a planar lipid bilayer. In both cases, the surface is TiO_2 and liposomes were made of dioleoyl phosphatidyl choline (red curves) and dioleoyl phosphatidyl choline containing 20% of dioleoyl phosphatidyl serine (blue curves). The differences between the two cases are quite striking: the liposome film causes a greater frequency shift than a bilayer. This happens because it is thicker. It also dissipates more energy, because it is laterally heterogeneous. Gaining further information about the transition region (blue curves, 0–8 min), where liposomes and bilayers coexist on the interface, requires both additional measurements of the total lipid mass by an independent technique on the same surface and further modeling. Viscoelastic model has been routinely applied to this system, but the veracity of its results has to be very carefully re-examined in light of the recent work on laterally heterogeneous films. Details of liposome behavior at inorganic surfaces have recently been reviewed in ref 19.

The availability of simple-to-use, essentially “turn-key”, systems with exquisite control of the relevant experimental variables (crystal mounting, fluid exchange,⁵¹ and temperature) developed by Q-Sense paved the way for extensive application of this technique in the area of biointerfaces.^{1,9,27} The key advantage offered by QCM in this context is its sensitivity to the organization of the material at the interface. For example, it is notoriously difficult, by optical mass-sensitive techniques such as SPR or ellipsometry, to distinguish a layer of adsorbed liposomes from a flat lipid bilayer. The same distinction is trivial by QCM (Figure 3) without any further quantitative analysis even if the amount of lipid material at the surface is the same in both cases.¹¹ This ability to distinguish between liposomes and bilayers,¹¹ smooth layers of monomeric protein and piles of aggregates,³⁸ monomeric and clustered membrane-bound proteins,²⁸ straight, kinked, and looped surface-grafted DNA molecules,²⁴ and so on, is strong incentive for using QCM.

While qualitative analysis of QCM data may be as simple as shown in Figure 3, quantification of frequency and bandwidth shifts acquired on several overtones in terms of film-specific parameters requires an adequate understanding of the mechanical and hydrodynamic phenomena at play. Several approaches to quantitative interpretation of QCM data on thin films have been presented in the literature. Until now, the most common approach relied on a continuum model, where the sample properties are parametrized by a set of one or more slabs with certain thicknesses,

Table 1. Overview of the Approaches to QCM Data Interpretation

type of film	dissipative response	QCM data interpretation	
		approach	output
laterally homogeneous film	$\Delta\Gamma_n \ll -\Delta f_n$, or ^a low dispersion in $\Delta f_n/n$	Sauerbrey equation	<ul style="list-style-type: none"> areal mass density (may include solvent inside the film)
	$\Delta D > 0$	viscoelastic model	<ul style="list-style-type: none"> areal mass density (may include solvent inside the film) viscoelastic properties (frequency dependent loss and storage moduli or compliances)
		intrinsic viscosity	<ul style="list-style-type: none"> $\Delta\Gamma_n/-\Delta f_n$ ratio has been used to obtain structural information about the molecules in the film.²⁴
monolayer of discrete particles or other nanosized objects	ΔD is small, or ^a low dispersion in $\Delta f_n/n$	Sauerbrey equation	<ul style="list-style-type: none"> areal mass density (including liquid inside the film)
		empirical trapped-liquid coat model	<ul style="list-style-type: none"> areal mass density of trapped liquid particle size and height-to-width ratio lateral distribution of particles (clustering)
	$\Delta D \geq 0$	FEM simulation of hydro-dynamics	<ul style="list-style-type: none"> local mechanical properties (linker stiffness) in principle also particle size, shape and coverage. Quantitative predictions limited by computational resources.
		model-independent	<ul style="list-style-type: none"> $\Delta\Gamma_n/-\Delta f_n$ ratio has been used to obtain adsorbed particle size in a model-independent fashion²⁶

^a Either of the two criteria can be applied, though the criteria of low dispersion in $\Delta f_n/n$ is more stringent.

densities and mechanical (viscoelastic) properties.⁸ This approach is rooted in the work on torsional resonators done in the 1940s^{40,41,46} and is appropriate for homogeneous films, in which the length scale of the sample's internal structure is smaller than the film thickness and the wavelength of sound. It is not appropriate for films consisting of discrete particles (proteins, liposomes, viruses) adsorbed on the surface, where the film thickness is about the same as particle diameter and attachment to the substrate is of

much importance. Indeed such films behave differently: we have recently identified a new dissipation mechanism operating in these films that is not captured by the continuum model.^{26,35–38,52} Other approaches include the work on porous and rough films by Urbakh and colleagues,⁵³ which however does not explain significant dissipation typically observed in biomacromolecular films on surfaces.⁵⁴ In a different tack on the effective medium approximation, Gizeli and colleagues related QCM

response to the intrinsic viscosity of the adsorbates and extracted shape and size of surface-grafted DNA molecules.²⁴ The concept of intrinsic viscosity is borrowed from colloidal physics, where viscosity change (here, the change in frequency and dissipation) upon addition of colloidal particles depends on particle shape. On the other hand, Vörös et al.¹⁷ and Okahata et al.⁵⁵ correlated energy dissipation observed by QCM with the solvent content of biomolecular films, a concept that receives a clear physical meaning in the context of the laterally heterogeneous films discussed below.³⁷

The above summary illustrates that on one hand, a number of attempts have been made over the years to provide alternatives to the viscoelastic model. Their goal was to obtain from QCM data practically relevant parameters characterizing interfacial films, such as particle size and molecular geometry. On the other hand, given the recent progress, there is a need to collect various approaches and guidelines for their application in a unified and accessible fashion.

In doing so, we had to limit the scope of this Feature Article somewhat. Several topics not included in it deserve a special mention. For reasons of space, clarity, and consistency, we do not discuss QCM work on cells. It is a rapidly growing and exciting field of QCM application with its own set of questions related to data interpretation that is worthy of a separate examination; the reader is referred to a number of reviews and original papers on this subject.^{12,30–33,56} Similarly, recent exciting work on QCMs operated at high amplitudes⁵⁷ is based on a different set of principles and requires different approaches to data interpretation. Another concept that we do not discuss in any detail is slip, that some authors suggest may be important.^{58,59}

Last but not least, the concepts enunciated here apply to other shear horizontal surface acoustic wave devices, such as torsional resonators,^{40,41,46,60} surface acoustic wave devices,^{61,62} magneto-acoustic resonators (MARS),⁶³ and so on.⁸

■ INTERPRETATION OF QCM DATA

Different types of films a researcher is likely to encounter are grouped in Table 1 and schematically depicted in Figure 2 according to their morphology and the observed dissipation response: they can either be laterally homogeneous (Figure 2A, C) or not (Figure 2B, D); in either case, they may or may not dissipate energy (Figure 2A, B vs C, D). In the following, we describe the characteristics of these films and the approaches to data interpretation for each of them. It turns out that the different approaches to QCM data interpretation for these different kinds of films rest on one unifying concept called the “small load approximation”. This paper concludes with the description of this concept.

Table 1 illustrates one important point that we will be returning to continuously throughout the text: in many cases, complementary information greatly facilitates quantitative interpretation of QCM data. In some cases, it is simply indispensable.

Laterally Homogeneous Films. Homogeneous films may either induce a small dissipation shift (Figure 2A) or a large one (Figure 2C). To make the distinction more quantitative, the ratio of $\Delta\Gamma/-\Delta f$ should be considered. If $\Delta\Gamma_n \ll -\Delta f_n$ (or equivalently $\Delta D_n/(-\Delta f_n/n) \ll 4 \times 10^{-7} \text{ Hz}^{-1}$ for a 5 MHz crystal), then the film can be approximated as rigid, and the Sauerbrey equation can be used to extract the areal mass density of the film. It should be born in mind that if the film is solvated, the areal mass density of the film will include the masses of the adsorbate,

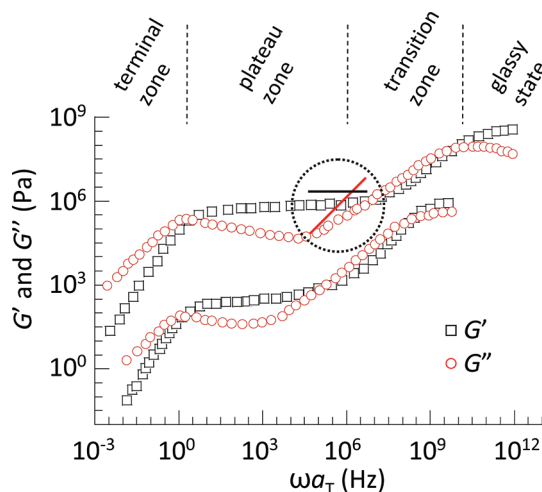


Figure 4. Linear rheological spectra of viscoelastic media. Plotted in this figure are the storage modulus G' (black) and the loss modulus G'' (red) for a long-chain linear polystyrene-butadiene copolymer melt (top curves, adapted from ref 71) and a polyisoprene melt (bottom curves, adapted from ref 87). The polyisoprene curves were shifted by 3 decades along the vertical axis for clarity. Spectra were acquired at frequencies accessible to conventional rheological equipment and later shifted on the frequency scale making use of the time–temperature superposition principle;⁷⁰ the x -axis is the product of angular frequency, ω , and a temperature-dependent shift factor, a_T . In long-chain polymers, stress relaxation processes fall into two classes, which are the segmental relaxations (fast) and the disentanglement processes (slow). The frequencies of these relaxations define the “zones”. In the terminal zone (on long time scales), the material flows like normal liquid (albeit with a viscosity much higher than that of water). The terminal zone is only observed if the material is not cross-linked. In the plateau zone, the mechanical response is dominated by cross-links and/or entanglements. Here, the material appears predominantly elastic ($G' > G''$) and the storage modulus is approximately constant. This zone is also called the “rubber plateau” and occurs in gels, polymer melts, as well as semidilute polymer solutions. In the transition zone the rheological response is dominated by the dynamics of individual network strands. G' and G'' have similar magnitude. In the glassy zone, the motion on the local scale dictates the rheological behavior. The dashed circle shows a frequency range, in which the material may arguably be described as a “Voigt-Kelvin material” (the slopes of $G'(\omega)$ and $G''(\omega)$ are 0 and 1, as indicated by the black and the red lines, respectively). “Linear” in the caption of this figure refers to the relationship between stress and strain. It is linear for small deformations that are typically relevant in QCM measurements.

m_{ads} and of the solvent, m_{solvent} in the film:

$$m_f = m_{\text{ads}} + m_{\text{solvent}} \quad (3)$$

If m_{ads} is available from an independent measurement, e.g., with a mass-sensitive optical technique such as surface plasmon resonance (SPR)⁶⁴ or ellipsometry,⁶⁵ the weight fraction of the solvent in the film can be quantified. Film thickness can be readily estimated through eq 1 if the densities of the adsorbate, ρ_{ads} , and of the solvent, ρ_{solvent} , are similar. If the densities are different, the following relationship can be used, but m_{ads} needs to be measured independently:³⁴

$$h_f = \frac{1}{\rho_{\text{solvent}}} \left[m_f - m_{\text{ads}} \left(1 - \frac{\rho_{\text{solvent}}}{\rho_{\text{ads}}} \right) \right] \quad (4)$$

If $\Delta D > 0$, then the film is sufficiently soft and sufficiently thick for the QCM to become sensitive to the mechanical or, more precisely, viscoelastic properties of the film.^{8,40,66–69} These properties are commonly represented by the complex shear modulus $G = G' + iG''$, where i is the imaginary unit (the square root of -1). Their measurement is the realm of rheology, hence QCM becomes a rheometer.

The storage modulus G' describes material elasticity, i.e., the relationship between applied force and the extent of deformation. It can be thought of as a spring constant. The loss modulus $G'' = \omega\eta$ describes viscous energy dissipation in the material subjected to deformation, where the viscosity η can be thought of as a friction coefficient that relates the applied force to the rate of deformation. A material exhibits predominantly elastic behavior if $G' \gg G''$ and predominantly viscous, if $G' \ll G''$. If $G' \approx G''$, it is viscoelastic. It is important to note that G' and G'' vary with the angular frequency of deformation ω and that these variations typically span many orders of magnitude (Figure 4). Within a limited frequency range, the dependencies are often well-approximated by power laws with exponents α' and α'' : $G'(\omega) = G_0'(\omega/\omega_0)^{\alpha'}$, $G''(\omega) = G_0''(\omega/\omega_0)^{\alpha''}$, where ω_0 is an arbitrarily chosen reference frequency. The exponents, and the frequencies at which they occur, are related to (and hence provide information about) microscopic interactions and motions within the sheared material (Figure 4).^{70,71}

The QCM response for laterally homogeneous viscoelastic films is successfully treated by a continuum model based on the analysis of shear wave propagation in viscoelastic media in much the same way as is done in optics for electromagnetic waves⁷² (recently reviewed by Johannsmann⁸). For thin films (film thickness much thinner than the wavelength of the shear-acoustic wave in the film), frequency and bandwidth shifts are related to the areal mass density of the film and its viscoelastic properties as follows:^{8,73}

$$\begin{aligned} \Delta f_n &\approx -\frac{n}{C} m_f \left(1 - n\omega_F \rho_l \eta_l \frac{G_f''}{\rho_f (G_f'^2 + G_f''^2)} \right) = -\frac{n}{C} m_f \left(1 - n\omega_F \rho_l \eta_l \frac{J_f'}{\rho_f} \right) \\ \Delta \Gamma_n &\approx \frac{n}{C} m_f n\omega_F \rho_l \eta_l \frac{G_f'}{\rho_f (G_f'^2 + G_f''^2)} = \frac{n}{C} m_f n\omega_F \rho_l \eta_l \frac{J_f''}{\rho_f} \end{aligned} \quad (5)$$

Here, subscripts l and f refer to the liquid and the film, respectively. $m_f = \rho_f h_f$ is as usual the areal mass density of the film, and $J = J' - iJ'' = G^{-1}$ is the frequency-dependent compliance of the film; J' and J'' are the elastic and viscous components of the compliance, respectively. Laterally homogeneous acoustically thin films whose density and mechanical properties continuously vary in the vertical direction can also be treated with this approach in a rigorous manner by assuming the form of the profile (block, exponential, or parabolic) and integrating the term in brackets on the right-hand side of eq 5 to predict Δf and $\Delta \Gamma$. This yields a well-defined equivalent thickness and z -averaged viscoelastic properties.⁷³ There are numerous examples of such films, with polymer brushes being the most common. Dedicated software for numerical fitting of QCM data in terms of film properties is available.⁷⁴

The application of the viscoelastic model requires a certain amount of care. It has five independent fitting parameters: the areal mass density $\rho_f h_f$, the shear moduli G' and G'' , which enter as products with density, $\rho_f G'$ and $\rho_f G''$, and the exponents α' and α'' describing the frequency dependence of the moduli (Figure 4). An assumption about film density ρ_f is required to

obtain film thickness and the actual values of the shear moduli, and independent knowledge of some of the film properties is helpful, if not essential, for a model with so many fitting parameters to provide meaningful results.

Film density ρ_f can be estimated if the density of the adsorbate and the solvent are similar or calculated from eq 4 if the film thickness and the areal adsorbate mass density are known. In soft matter, a reasonable assumption often is $\rho_f \approx 1 \text{ g/cm}^3$. Film thickness can be obtained from measurements with atomic force microscopy or reflection interference contrast microscopy.^{13,21,29} Note that while areal mass densities obtained by QCM can be compared with those obtained by optical mass-sensitive techniques (see eq 3),^{14,16,18,29} the comparison of film thicknesses between these techniques is a more complicated endeavor that goes beyond the scope of this Feature. The reader is referred to Domack et al.¹⁰ and Plunkett et al.¹⁵ who treat this subject in some detail (albeit differently).

Furthermore, when reporting results obtained by fitting the data with such complex models, it is important to establish confidence intervals that make it possible to assess the significance of the numbers generated by the fitting. The method described in Eisele et al.²⁹ provides an example of how this can be done.

It should be kept in mind that viscoelastic properties determined by QCM may differ substantially from those obtained with other rheometers (see Figure 4) because QCM measures at frequencies that exceed those employed in most conventional bulk rheometers by several orders of magnitude. It is therefore sensitive to microscopic relaxation processes within the film that occur at significantly shorter time scales.

Equation 5 is written in terms of the film shear modulus $G(\omega)$ as well as film compliance $J(\omega)$ to illustrate that QCM is more sensitive to the mechanical properties of the softer (more compliant) films than to those of the stiffer (less compliant) ones. This representation is particularly useful for thin films that are stiffer than the surrounding liquid and much thinner than the penetration depth of the shear wave in liquid $\delta = (2\eta_l / (2\pi n f_F \rho_l))^{0.5}$ (for water at 5 MHz ($n = 1$), $\delta \sim 250 \text{ nm}$). In this case, the dispersion in $\Delta f_n/n$ will be small, hence the second term in the brackets of eq 5 can be neglected and J' can be readily calculated from⁷⁵

$$\frac{\Delta \Gamma_n}{\Delta f_n} = -\frac{\rho_l n\omega_F \eta_l J_f''}{\rho_f} \quad (6)$$

A more general expression is derived for thicker films in ref 26. Equation 6 rationalizes how the ratio of $\Delta \Gamma$ (or ΔD) and Δf can provide useful information. A comparison with the work of Gizeli and co-workers²⁴ suggests a direct relationship between J' and intrinsic viscosity of the film components.

In the past, the so-called Voigt–Kelvin model has frequently been employed to interpret QCM-D data. This model is commonly attributed to Voinova et al.,⁷⁶ though actually it is a special case of earlier work (e.g., eq 7 in ref 10). This model assumes a frequency-independent G' and η (G'' in this model depends linearly on frequency since $G'' = \omega\eta$). As an example, the range where the Voigt–Kelvin model may be approximately valid for the textbook set of data taken from ref 71 is indicated with a dashed circle in Figure 4, but for most materials of interest, the Voigt–Kelvin range does not exist at all. Furthermore, in

practice, this frequency range is unlikely to coincide with the frequencies covered by QCM, except coincidentally.⁸ Moreover, coupling of the material to the surface of the QCM crystal leads to additional relaxations. In other words, assuming G' to be frequency independent and G'' to depend linearly on frequency represents an artificial limitation of the parameter space and usually is not justified.

Films of Discrete Nanosized Objects. There are numerous examples of films that consist of discrete nanosized objects: adsorbed globular proteins, liposomes, viruses, nanoparticles (Figure 2B,D). The implications of the lateral heterogeneity of this type of film for the data interpretation had not been considered until recently. Instead, it was assumed that they could be analyzed with the same viscoelastic model as the homogeneous films. The QCM response in laterally heterogeneous films, however, is governed by hydrodynamic effects and the motion of surface-adsorbed particles. We have shown that these can be modeled empirically³⁵ and understood fundamentally,^{36,37} changing the way QCM data is interpreted and paving the way for new applications.

The frequency response of particle films can be readily translated into the areal mass density using eq 1 if the variation in $\Delta f_n/n$ as a function of n (the overtone dispersion) is low. The areal mass density derived in this way contains contributions from liquid in the interior of the particles and in interstitial spaces between them. The extent of liquid trapping is governed by the hydrodynamics of the system and depends sensitively on the particles' surface coverage, size, shape, orientation, and lateral distribution. Combining in situ QCM with other techniques, such as optical reflectometry,³⁵ ellipsometry,^{10,28} surface plasmon resonance,^{77,78} or atomic force microscopy,^{36,38,79,80} has enabled the examination of the QCM response as a function of independently measured surface coverage. These studies clearly demonstrated that the frequency shift is not a linear function of the surface coverage. Instead, the relative contribution of the surrounding liquid to the frequency response decreases with increasing coverage, and the sensitivity of QCM to the adsorbing particles is disproportionately high at low coverage but disproportionately low at high coverage.

The case of high coverage is rather simple and converges with that of homogeneous films discussed above. Here, almost all of the liquid in the interstitial space contributes to the frequency shift, i.e., the areal mass density corresponds to the mass of all the material, particles and liquid, within a surface adlayer as thick as the particles are high.^{22,36,38} Particle height can in this case be readily estimated from eqs 1 or 4.²⁸ This trapping mechanism was discussed previously by Martin et al.⁸¹ and applied to studying thin (micellar) film morphology by Macakova et al.²² Similar ideas have been developed by Daikhin and Urbakh.⁵³

At lower coverage, the situation is more complex but can be rationalized in terms of coats of hydrodynamically trapped liquid that surround each adsorbed particle. These coats of hydrodynamically trapped liquid should not be confused with the hydration shells, i.e., the layer(s) of solvent molecules that surround solutes or surfaces and that exhibit dynamics and/or order different from the bulk solvent molecules. Their overlap provides an intuitive explanation for the decrease in sensitivity upon filling a monolayer with particles. Examining the process of particle adsorption in Figure 5B, it is clear that a particle adsorbing in a crevice between two previously adsorbed particles contributes a smaller mass than the same particle adsorbing to the bare surface. Of course there is no sharp line separating

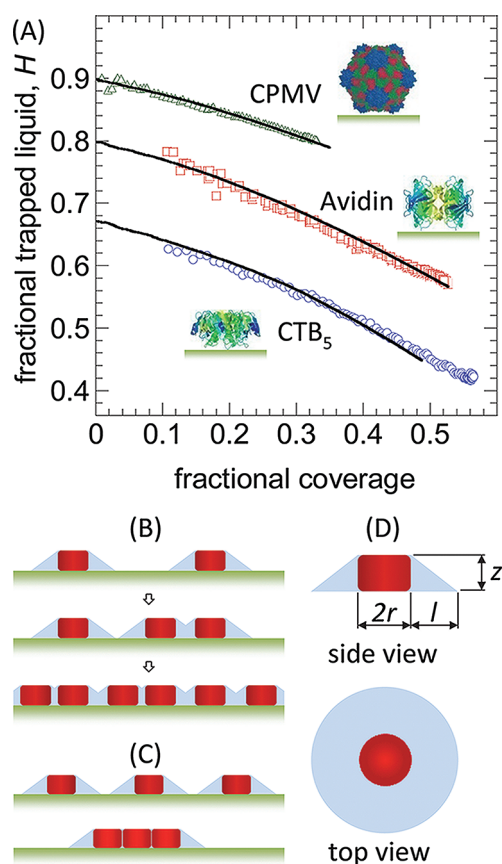


Figure 5. Solvent contribution to the QCM response depends on coverage. (A) Selected plots of the fractional trapped liquid $H = 1 - m_{\text{ads}}/m_f$ (i.e., the contribution of the liquid to the areal mass density measured by QCM) against the fractional surface coverage, determined from combinations of optical mass-sensitive techniques (reflectometry or ellipsometry)^{28,35} with QCM for the adsorption of particles of various sizes and height-to-width ratios: cowpea mosaic virus (CPMV; green triangles), cholera toxin B₅ subunit (CTB₅; blue circles) and avidin (red squares). The particles' structure and orientation on the surface are also shown (insets; CPMV has a diameter of 28 nm. For clarity, sizes of CTB₅ and avidin are enlarged 4-fold with respect to CPMV). Generally, the fractional trapped liquid and the rate of its decrease with coverage are sensitive to the particles' height-to-width ratio and internal liquid content. Compact and flat particles, such as CTB₅, contain little trapped liquid. Particles with large solvent-filled cavities or lower height-to-width ratios, such as CPMV, contain more trapped liquid. Lines are fits to the data with the trapped-liquid coat model. The parameters of the model are described in detail in parts B–D. (B) Phenomenologically, the trapped liquid can be rationalized as a coat (light blue) that surrounds each adsorbed molecule (red). With increasing coverage, these coats increasingly overlap, leading to a decrease in the fractional trapped liquid. (C) The amount of trapped liquid also depends on the lateral organization of surface-bound material. A compact cluster traps less liquid than if the particles were dispersed homogeneously across the surface. In this way, the measured areal mass density becomes sensitive to the lateral organization of surface-bound material.²⁸ (D) To fit the data shown in part A, particles were modeled as upright rigid cylinders carrying liquid coats with the shape of truncated cones. It was further assumed that the particles were randomly distributed on the surface. Fitting experimental data (black lines in part A) with z and l as free parameters yields $l/z = 1.35 \pm 0.15$. The steepness l/z of the coat is independent of the particle size (sizes up to 30 nm were tested) and height-to-width ratio (ratios between 0.3 and 1 were tested).²⁸ To what extent these simple geometrical assumptions work for particles with arbitrary shape is subject to discussion and needs further research.

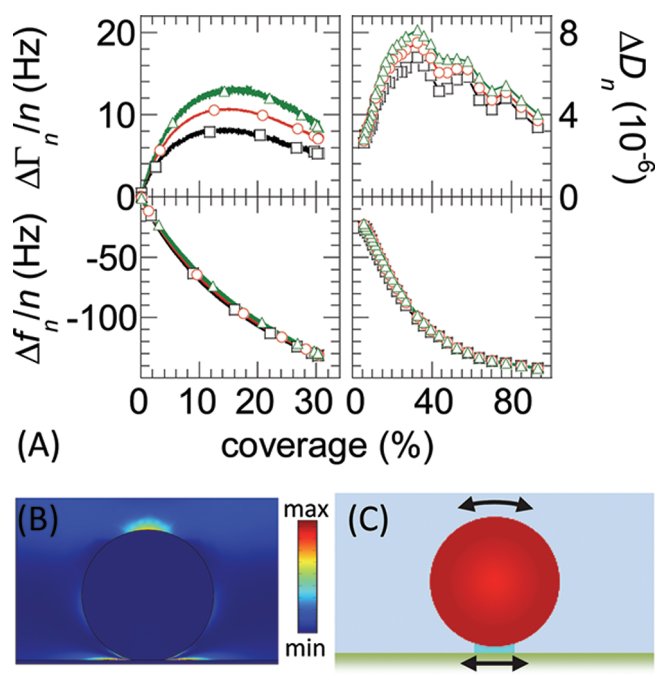


Figure 6. Laterally heterogeneous films, experimental data and FEM simulations. (A) Left: QCM response for a CPMV monolayer as a function of coverage. Colors represent different overtones ($n = 5, 9,$ and 13). Frequency shifts are very similar for all overtones n and are not linear in coverage. The dissipation shifts show a pronounced maximum. Right: FEM simulations that capture the hydrodynamics and the mechanics of the experimental situation reproduce the main experimental features: the nonlinear relationship between the coverage and the frequency shifts and the maximum in the dissipation. The difference in the location of the maximum and the weak undulations in ΔD result from relying on a two-dimensional periodic array of adsorbed particles (using cylinders instead of spheres) rather than a random distribution of adsorbed spheres in 3D for computational reasons. For details see refs 36 and 37. Note, that the cylinders in this simulation were rather stiff: a homogeneous film with the same stiffness and thickness would exhibit a dissipation shift of only $\sim 0.6 \times 10^{-6}$. (B) Map of the energy dissipation in and around an oscillating particle. Most of the dissipation arises at the liquid-particle boundary.³⁷ (C) The FEM simulations have shown that most of the dissipation originates from nm-scale rotational (“rocking”) and translation (“sliding”) motion (black arrows) of the particles (red) pivoted around the contact region (turquoise). The extent of motion depends on the compliance of the contact region (also called linker).

trapped solvent from free solvent, but these coats are a useful approximation to the complex hydrodynamic effects that come into play in these films. An empirical model assuming that the shape of the liquid coat around each adsorbed particle is fixed, and that particles are randomly distributed on the surface (cf. random sequential adsorption),⁸² has proven remarkably successful in quantitatively reproducing coverage-dependent frequency responses (Figure 5).^{28,35} The trapped liquid coat model relies on an independent measurement of the areal mass density of the adsorbate m_{ads} (see eq 3), e.g., with reflectometry or ellipsometry. The fractional trapped liquid ($H = 1 - m_{\text{ads}}/m_f$) vs m_{ads} data, where m_f is obtained by QCM, is then fitted. If particle weight and lateral distribution are known, the fit yields particle size and height-to-width ratio. If the particle size and orientation on the surface are known, the fit provides information about the lateral distribution of particles, such as the degree of clustering (e.g., protein oligomerization).^{28,83}

The same problem was also approached from a more fundamental perspective. Hydrodynamic effects in QCM were modeled explicitly by finite element method (FEM) simulations in which the stress distribution around the surface-bound particles was calculated and used to derive the frequency and dissipation changes (Figure 6).^{36,37} With molecular geometry and mechanical parameters as a starting point, these rigorous simulations reproduced the coverage-dependent decrease in sensitivity of QCM in laterally heterogeneous films (Figure 6A) without the need for fitting parameters.³⁶ One interesting point emerging from these studies, that could be exploited in applications, is that QCM is much more sensitive at low coverage where the hydrodynamic effects are the strongest, overestimating the adsorbed mass by as much as a factor of 10.^{16,35,38}

Importantly, FEM simulations provided essential insight into the QCM response by identifying a previously unknown pathway of energy dissipation that is fundamentally different from those operating in homogeneous films:^{36,37} most of the energy is dissipated at the liquid-particle boundary (Figure 6B), but the amount of dissipation strongly depends on the stiffness of the particle-surface contact (Figure 6C) and on the surface coverage.

The sensitivity to the particle-surface contact stiffness arises because particles attach to surfaces via narrow linker or contact zones (Figure 6C). FEM simulations showed that particles essentially act as lever arms pivoted around the linkers as they are moved through the liquid by the oscillating crystal. In fact, because the stress is concentrated at the link, adsorbed particles can deform even rather stiff contact zones. For this reason, even films of very stiff particles will dissipate some energy, while a homogeneous film of the same stiffness will not.³⁶ In this way, the QCM becomes very sensitive to the mechanical properties of linkers, such as hinge regions in proteins, and should hence be uniquely suited to interrogate them.

The dependence on the surface coverage comes about because neighboring particles, when close enough, shield each other from the effects of flow. This effect is responsible for the observation of transient peaks in dissipation in many systems (Figure 6A)³⁷ that were previously attributed to various conformational or phase transitions.

The linker-dependent pathway of energy dissipation appears to be dominant in laterally heterogeneous films but is neglected in the continuum viscoelastic model that describes homogeneous films. The assumption of lateral homogeneity that is key to the application of the viscoelastic model is violated. It is therefore not useful to apply the viscoelastic model to monolayers of globular proteins or any other discrete nanoscale particles. For example, application of the viscoelastic model to a virus particle monolayer (left panel in Figure 6A; at maximal coverage and assuming a realistic film thickness of 28 nm) would result in $|G| \approx 175$ kPa at 5 MHz, which is almost 20-fold less than the value used in the corresponding FEM simulations³⁷ (right panel in Figure 6A).

How does one distinguish between the different types of layers in practice? In that regard, experiments and FEM simulations have shown a linear decrease of the $\Delta\Gamma_n/-\Delta f_n$ ratio as a function of $-\Delta f_n/n$ for the adsorption of discrete objects to surfaces, with an overtone-independent intercept in the limit of $\Delta\Gamma_n/-\Delta f_n = 0$.^{26,37} It is not clear why this decrease should be linear. A different response is predicted by the viscoelastic model for homogeneous films. Indeed, this has been observed in some cases in polymer films and was used to extract structural information about the molecules comprising the films.²⁴ Further theoretical and

experimental efforts are needed to investigate whether this can be used as a tool to distinguish between laterally homogeneous and laterally heterogeneous films and to establish the physical basis underlying the observations. Clearly, research into the physical phenomena underlying such characteristic responses will generate improved interpretational approaches and enable entirely novel sensing applications.

Small Load Approximation: Constructing Models for QCM Data Interpretation for Different Interfaces. With the four different types of films presented in Table 1 and different approaches to data interpretation just described, an inquisitive reader may wonder if there is a unifying theme or principle underlying this diversity. Indeed there is. Introducing a complex frequency shift $\Delta f^* = \Delta f + i\Delta\Gamma$,⁸⁴ one can write $\Delta f^* = iZ_L/(2\pi m_q)$, where m_q is the areal mass density of the quartz crystal and $Z_L = Z_L' + iZ_L''$ is the ratio of shear stress-to-velocity at the oscillating crystal surface. This quantity is called the "load impedance".⁴⁷ The linear relationship between the frequency shift and the load impedance is called the small load approximation. To our knowledge, it was first introduced by Borovikov in his paper on the measurement of liquid viscosity with QCM.⁴⁷ Considering that stress is force per unit area, QCM can be thought of as a force balance.

For laterally homogeneous films, load impedance can be straight-forwardly calculated using Fresnel theory borrowed from optics,^{65,72} as discussed in more detail in refs 8 and 67. The role of the refractive index is played by the acoustic impedance of the material, $Z = (\rho G)^{1/2}$.⁶⁷ In the case of very stiff materials (large G' and $G' \gg G''$) or very thin films, one has $Z_L = i\omega m$, leading to a frequency shift that is real (zero dissipation), in other words, the Sauerbrey relationship, eq 1. Otherwise the same calculation leads to complex frequency shifts (nonzero dissipation, eq 5). This is indeed the origin of the criterion $\Delta\Gamma \ll -\Delta f$ that was used above to determine if the Sauerbrey relationship could be applied; otherwise, neglecting the imaginary part of the frequency shift (the dissipation) introduces large errors.

For heterogeneous films, the area-averaged stress has to be calculated numerically, for example, by averaging the shear stress obtained through the FEM simulations over the interface. Dividing by the velocity of the surface (a known quantity) yields shifts in the bandwidth and in the frequency, such as those presented in Figure 6. The modeling is quantitative but computationally demanding. Further research is needed to extend it to a set of suitably simple but still realistic geometries characteristic of the various ways in which adsorbed objects may behave.

A particularly striking example of heterogeneous samples are micrometer-sized particles attached to the crystal surface. Positive frequency shifts observed in this system can be straight-forwardly understood within the framework of the QCM as a force balance in terms of the stiffness of the sphere/crystal contact.^{85,86} In contrast, such positive frequency shifts would be impossible according to the conventional perception of the QCM as a mass balance.

CONCLUDING REMARKS

QCM has been instrumental in biointerface research thanks to its ability to operate in liquids, a condition that is crucial for biological samples, and to provide a wealth of information about interface organization. In this Feature, we have described the physical mechanisms underlying the ability of QCM to probe the organization of solid–liquid interfaces and hopefully given the users of this technique the necessary conceptual tools for

interpreting their data. Specifically, focusing on dissipative processes in the film, we distinguish between films that do not dissipate energy and can be dealt with using the Sauerbrey relationship and films that do dissipate energy and require a different approach. These latter films come in two varieties: laterally homogeneous, where dissipation arises from molecular motions inside the film, and laterally heterogeneous on the scale of the film thickness, where the dissipation arises predominantly from the motion of particles and occurs at the liquid–particle boundary. Recent research makes it clear that data interpretation strategies for these two films are different. Recognizing these differences enables quantitative interpretation of QCM data and opens new possibilities for sensing applications and basic research. The idea of QCM as a force balance allows the unified treatment of all of these cases within the framework of the small load approximation based on the calculation of the stress at the surface.

Finally, the overview in Table 1 illustrates that the quantitative interpretation of QCM data alone is severely limited. A lot of additional information can be obtained by the combination of QCM with another method that can determine the mass of the adsorbate per surface area.

AUTHOR INFORMATION

Corresponding Author

*Ilya Reviakine: e-mail, ireviakine@cicbiomagune.es; phone, +34 943 00 53 12; fax, +34 943 00 53 15. Ralf Richter: e-mail, rrichter@cicbiomagune.es; phone, +34 943 00 53 29; fax, +34 943 00 53 15.

BIOGRAPHY

Dr. Ilya Reviakine studied Biochemistry at McMaster University (Ontario, Canada) as an undergraduate and received his Ph.D. in Mathematics and Natural Sciences from the University of Groningen (The Netherlands), where he worked with Prof. Alain Brisson on atomic force microscopy of biological macromolecules and their assemblies. He did his postdoctoral work first in the area of biointerfaces at the Swiss Federal Institute of Technology (ETH) in Zürich (Switzerland) and then in the area of protein crystallization at the University of Houston (TX). In 2005 he received an Alexander von Humboldt Research fellowship to work with Prof. Diethelm Johannsmann on the shear-acoustic response in laterally heterogeneous ultrathin films at the Clausthal University of Technology (Germany). In October 2006, he joined CIC biomaGUNE (San Sebastian, Spain) as a Group leader. His research on bio/nonbio interfaces primarily focuses on lipidic systems (surface-adsorbed liposomes and supported bilayers, effects interactions with foreign surfaces have on membranes of cells, organization of transmembrane proteins at solid/liquid interfaces), and on blood-biomaterial interactions. Professor Diethelm Johannsmann studied physics in Bonn and Heidelberg (Germany) and obtained his Ph.D. degree from Mainz University (Germany) in 1991, working on the use of quartz resonators to study of soft interfaces. After a postdoc at UC Berkeley (CA), where he worked on optical second harmonic generation, he joined the Max-Planck-Institute for Polymer Research at Mainz (Germany), studying polymers at interfaces with a number of different techniques. Since 2002 he is professor of Physical Chemistry at Clausthal University of Technology (Germany). His research interests are acoustic sensing, polymers at interfaces, organic coatings, and surface attached polymer gels.

Dr. Ralf Richter is Research Group Leader at the CIC biomacromolecule (San Sebastian, Spain) and at the Max Planck Institute for Intelligent Systems (Stuttgart, Germany). He obtained his MSc in Physics at Chalmers/Gothenburg University (Sweden) in 1999. He completed his Ph.D. in Chemistry at the IECB/University of Bordeaux (France) in 2004, where he worked on the characterization of biomolecular self-assembly at interfaces (formation of supported lipid bilayers, two-dimensional crystallization of proteins). During a postdoctoral stay at the University of Heidelberg (Germany) until 2007, he initiated work on self-assembly phenomena of pericellular matrixes that are rich in the carbohydrate hyaluronan. Current research revolves around soft biological structures at interfaces, such as lipid membranes, pericellular matrixes, or the nuclear pore complex. His research group creates and interrogates well-controlled biomimetic model systems with tunable complexity to understand the physical principles underlying the self-organization, structure, and function of these architectures and for applications as biosensors and for the control of cellular fate.

ACKNOWLEDGMENT

We would like to thank Michael Rodal, Nico Eisele, and Marta Gallego for critical reading of the manuscript. R.P.R. and I.R. gratefully acknowledge funding from the Department of Industry of the Basque Government (Program ETORTEK) and from the Spanish Ministry of Science and Innovation (MICINN, Grants MAT2008-04192 and RYC2009-04275 to R.P.R. and Grant CTQ2009-11245 to I.R.). R.P.R. furthermore acknowledges funding from the German Federal Ministry of Education and Research (BMBF, Grant 0315157). D.J. acknowledges funding by the Deutsche Forschungsgemeinschaft under Contract Jo 278/12-1.

REFERENCES

- Hook, F.; Kasemo, B.; Grunze, M.; Zauscher, S. *ACS Nano* **2008**, *2*, 2428–2436.
- Kasemo, B. *Surf. Sci.* **2002**, *500*, 656–677.
- Fusetani, N. *Nat. Prod. Rep.* **2004**, *21*, 94–104.
- Fendler, J. H. *Chem. Mater.* **1996**, *8*, 1616–1624.
- Ward, M. D.; Buttry, D. A. *Science* **1990**, *249*, 1000–1007.
- Schumacher, R. *Angew. Chem., Int. Ed.* **1990**, *29*, 329–343.
- Marx, K. A. *Biomacromolecules* **2003**, *4*, 1099–1120.
- Johannsmann, D. *Phys. Chem. Chem. Phys.* **2008**, *10*, 4516–4551.
- Rodahl, M.; Hook, F.; Krozer, A.; Brzezinski, P.; Kasemo, B. *Rev. Sci. Instrum.* **1995**, *66*, 3924–3930.
- Domack, A.; Prucker, O.; Ruhe, J.; Johannsmann, D. *Phys. Rev. E* **1997**, *56*, 680–689.
- Keller, C. A.; Kasemo, B. *Biophys. J.* **1998**, *75*, 1397–1402.
- Zhou, T.; Marx, K. A.; Warren, M.; Schulze, H.; Braunhut, S. J. *Biotechnol. Prog.* **2000**, *16*, 268–277.
- Picart, C.; Lavalle, P.; Hubert, P.; Cuisinier, F. J. G.; Decher, G.; Schaaf, P.; Voegel, J. C. *Langmuir* **2001**, *17*, 7414–7424.
- Hook, F.; Kasemo, B.; Nylander, T.; Fant, C.; Sott, K.; Elwing, H. *Anal. Chem.* **2001**, *73*, 5796–5804.
- Plunkett, M. A.; Wang, Z. H.; Rutland, M. W.; Johannsmann, D. *Langmuir* **2003**, *19*, 6837–6844.
- Larsson, C.; Rodahl, M.; Hook, F. *Anal. Chem.* **2003**, *75*, 5080–5087.
- Voros, J. *Biophys. J.* **2004**, *87*, 553–561.
- Su, X. D.; Wu, Y. J.; Knoll, W. *Biosens. Bioelectron.* **2005**, *21*, 719–726.
- Richter, R. P.; Berat, R.; Brisson, A. R. *Langmuir* **2006**, *22*, 3497–3505.
- Ozeki, T.; Morita, M.; Yoshimine, H.; Furusawa, H.; Okahata, Y. *Anal. Chem.* **2007**, *79*, 79–88.
- Richter, R. P.; Hock, K. K.; Burkhartsmeyer, J.; Boehm, H.; Bingen, P.; Wang, G. L.; Steinmetz, N. F.; Evans, D. J.; Spatz, J. P. *J. Am. Chem. Soc.* **2007**, *129*, 5306–5307.
- Macakova, L.; Blomberg, E.; Claesson, P. M. *Langmuir* **2007**, *23*, 12436–12444.
- Malmstrom, J.; Agheli, H.; Kingshott, P.; Sutherland, D. S. *Langmuir* **2007**, *23*, 9760–9768.
- Tsartos, A.; Papadakis, G.; Mitsakakis, K.; Melzak, K. A.; Gizeli, E. *Biophys. J.* **2008**, *94*, 2706–2715.
- Steinmetz, N. F.; Bock, E.; Richter, R. P.; Spatz, J. P.; Lomonosoff, G. P.; Evans, D. J. *Biomacromolecules* **2008**, *9*, 456–462.
- Tellechea, E.; Johannsmann, D.; Steinmetz, N. F.; Richter, R.; Reviakine, I. *Langmuir* **2009**, *25*, 5177–5184.
- Cho, N. J.; Frank, C. W.; Kasemo, B.; Hook, F. *Nat. Protoc.* **2010**, *5*, 1096–1106.
- Carton, I.; Brisson, A. R.; Richter, R. P. *Anal. Chem.* **2010**, *82*, 9275–9281.
- Eisele, N. B.; Frey, S.; Piehler, J.; Gorlich, D.; Richter, R. P. *EMBO Rep.* **2010**, *11*, 366–372.
- Janshoff, A.; Kunze, A.; Michaelis, S.; Heitmann, V.; Reiss, B.; Wegener, J. *J. Adhes. Sci. Technol.* **2010**, *24*, 2079–2104.
- Marxer, C. M.; Coen, M. C.; Greber, T.; Greber, U. F.; Schlapbach, L. *Anal. Bioanal. Chem.* **2003**, *377*, 578–586.
- Wegener, J.; Janshoff, A.; Steinem, C. *Cell Biochem. Biophys.* **2001**, *34*, 121–151.
- Marx, K. A. In *Springer Series on Chemical Sensors and Biosensors*; Steinem, C., Janshoff, A., Eds.; Springer: Heidelberg, Germany, 2007; Vol. 5V, p 371.
- Hook, F.; Voros, J.; Rodahl, M.; Kurrat, R.; Boni, P.; Ramsden, J. J.; Textor, M.; Spencer, N. D.; Tengvall, P.; Gold, J.; Kasemo, B. *Colloid Surf. B* **2002**, *24*, 155–170.
- Bingen, P.; Wang, G.; Steinmetz, N. F.; Rodahl, M.; Richter, R. P. *Anal. Chem.* **2008**, *80*, 8880–8890.
- Johannsmann, D.; Reviakine, I.; Rojas, E.; Gallego, M. *Anal. Chem.* **2008**, *80*, 8891–8899.
- Johannsmann, D.; Reviakine, I.; Richter, R. P. *Anal. Chem.* **2009**, *81*, 8167–8176.
- Rojas, E.; Gallego, M.; Reviakine, I. *Anal. Chem.* **2008**, *80*, 8982–8990.
- Cady, W. G. *Piezoelectricity*; McGraw-Hill Book Company, Inc.: New York, 1946.
- Mason, W. P. *Piezoelectric Crystals and Their Application to Ultrasonics*; D. Van Nostrand Company, Inc.: New York, 1950.
- Mason, W. P.; Baker, W. O.; McSkimin, H. J.; Heiss, J. H. *Phys. Rev.* **1949**, *75*, 936–946.
- Beck, R.; Pittermann, U.; Weil, K. G. *Ber. Bunsen-Ges. Phys. Chem. Chem. Phys.* **1988**, *92*, 1363–1368.
- Ogi, H.; Motoshisa, K.; Matsumoto, T.; Hatanaka, K.; Hirao, M. *Anal. Chem.* **2006**, *78*, 6903–6909.
- Ogi, H.; Naga, H.; Fukunishi, Y.; Hirao, M.; Nishiyama, M. *Anal. Chem.* **2009**, *81*, 8068–8073.
- Sauerbrey, G. *Z. Phys.* **1959**, *155*, 206–222.
- Mason, W. P. *J. Colloid Sci.* **1948**, *3*, 147–162.
- Borovikov, A. P. *Instrum. Exp. Tech.* **1976**, *19*, 223–224.
- Kanazawa, K. K.; Gordon, J. G. *Anal. Chem.* **1985**, *57*, 1770–1771.
- Stockbridge, C. D. In *Vacuum Microbalance Techniques*; Behrndt, K., Ed; Plenum Press: New York, 1966; Vol. 5, p 193.
- Schillin, H.; Pechhold, W. *Acustica* **1969**, *22*, 244.
- Hermens, W. T.; Benes, M.; Richter, R.; Speijer, H. *Biotechnol. Appl. Biochem.* **2004**, *39*, 277–284.
- Edvardsson, M.; Svedhem, S.; Wang, G.; Richter, R.; Rodahl, M.; Kasemo, B. *Anal. Chem.* **2009**, *81*, 349–361.
- Urbakh, M.; Tsionsky, V.; Gileadi, E.; Daikhin, L. In *Piezoelectric Sensors*, 1st ed.; Steinem, C., Janshoff, A., Eds.; Springer: Heidelberg, Germany, 2006; pp 111–149.

- (54) Rodahl, M.; Hook, F.; Fredriksson, C.; Keller, C. A.; Krozer, A.; Brzezinski, P.; Voinova, M.; Kasemo, B. *Faraday Discuss.* **1997**, *107*, 229–246.
- (55) Manaka, Y.; Kudo, Y.; Yoshimine, H.; Kawasaki, T.; Kajikawa, K.; Okahata, Y. *Chem. Commun.* **2007**, *34*, 3574–3576.
- (56) Busscher, H. J.; Norde, W.; Sharma, P. K.; van der Mei, H. C. *Curr. Opin. Colloid Interface Sci.* **2010**, *15*, 510–517.
- (57) Cooper, M. A.; Dultsev, F. N.; Minson, T.; Ostanin, V. P.; Abell, C.; Klenerman, D. *Nat. Biotechnol.* **2001**, *19*, 833–837.
- (58) Ferrante, F.; Kipling, A. L.; Thompson, M. *J. Appl. Phys.* **1994**, *76*, 3448–3462.
- (59) Du, B. Y.; Goubaidouline, E.; Johannsmann, D. *Langmuir* **2004**, *20*, 10617–10624.
- (60) Bucking, W.; Du, B.; Turshatov, A.; Konig, A. M.; Reviakine, I.; Bode, B.; Johannsmann, D. *Rev. Sci. Instrum.* **2007**, *78*, 074903–1–8.
- (61) Lange, K.; Rapp, B. E.; Rapp, M. *Anal. Bioanal. Chem.* **2008**, *391*, 1509–1519.
- (62) Gronewold, T. M. A. *Anal. Chim. Acta* **2007**, *603*, 119–128.
- (63) Stevenson, A. C.; Lowe, C. R. *Sens. Actuators, A: Phys.* **1999**, *72*, 32–37.
- (64) Homola, J. *Anal. Bioanal. Chem.* **2003**, *377*, 528–539.
- (65) Azzam, R. M. A., Bashara, N. M. *Ellipsometry and Polarized Light*, 3rd ed.; Elsevier Science BV: Amsterdam, The Netherlands, 1996.
- (66) Martin, S. J.; Frye, G. C. In *IEEE 1991 Ultrasonics Symposium: Proceedings, Vols. 1 and 2*; McAvoy, B. R., Ed.; 1991; pp 393–398.
- (67) Johannsmann, D.; Mathauer, K.; Wegner, G.; Knoll, W. *Phys. Rev. B* **1992**, *46*, 7808–7815.
- (68) Bandey, H. L.; Martin, S. J.; Cernosek, R. W.; Hillman, A. R. *Anal. Chem.* **1999**, *71*, 2205–2214.
- (69) Lucklum, R.; Behling, C.; Cernosek, R. W.; Martin, S. J. *J. Phys. D: Appl. Phys.* **1997**, *30*, 346–356.
- (70) Ferry, J. D. *Viscoelastic Properties of Polymers*, 3rd ed.; Wiley & Sons: New York, 1980.
- (71) Oswald, P. *Rheophysics-The Deformation and Flow of Matter*; Cambridge University Press: Cambridge, U.K., 2009.
- (72) Heavens, O. S. *Optical Properties of Thin Solid Films*; Butterworth: London, 1955.
- (73) Johannsmann, D. *Macromol. Chem. Phys.* **1999**, *200*, 501–516.
- (74) The software QTM is freely available for download (http://www2.pc.tu-clausthal.de/dj/software_en.shtml), with a tutorial and guide, and contains the algorithms described in <http://www.pc.tu-clausthal.de/en/research/johannsmann-group/qcm-modelling/>; certain types of roughness effects are also implemented based on the work by Urbakh and co-workers. (Daikhin, L.; Gileadi, E.; Katz, G., et al. *Anal. Chem.* **2002**, *74* (3), 554). The software QTools is available from QSense and contains a viscoelastic model (small load approximation with a linear or a power-law frequency dependence of G' and G''); certain types of kinetic data analysis are also implemented.
- (75) Du, B. Y.; Johannsmann, D. *Langmuir* **2004**, *20*, 2809–2812.
- (76) Voinova, M. V.; Rodahl, M.; Jonson, M.; Kasemo, B. *Phys. Scr.* **1999**, *59*, 391–396.
- (77) Laschitsch, A.; Menges, B.; Johannsmann, D. *Appl. Phys. Lett.* **2000**, *77*, 2252–2254.
- (78) Reimhult, E.; Larsson, C.; Kasemo, B.; Hook, F. *Anal. Chem.* **2004**, *76*, 7211–7220.
- (79) Choi, K. H.; Friedt, J. M.; Frederix, F.; Campitelli, A.; Borghs, G. *Appl. Phys. Lett.* **2002**, *81*, 1335–1337.
- (80) Bund, A.; Schneider, O.; Dehnke, V. *Phys. Chem. Chem. Phys.* **2002**, *4*, 3552–3554.
- (81) Martin, S. J.; Frye, G. C.; Ricco, A. J.; Senturia, S. D. *Anal. Chem.* **1993**, *65*, 2910–2922.
- (82) Tarjus, G.; Schaaf, P.; Talbot, J. J. *J. Chem. Phys.* **1990**, *93*, 8352–8360.
- (83) A MATLAB routine to predict the coverage dependent contribution of liquid to the areal mass density as a function of the particle size, mass and aspect ratio, and for a selected set of lateral distribution scenarios is freely available for download, under www.rrichter.net.
- (84) Eggers, F.; Funck, T. *J. Phys. E* **1987**, *20*, 523–530.
- (85) Pomorska, A.; Shchukin, D.; Hammond, R.; Cooper, M. A.; Grundmeier, G.; Johannsmann, D. *Anal. Chem.* **2010**, *82*, 2237–2242.
- (86) Dybwad, G. L. *J. Appl. Phys.* **1985**, *58*, 2789–2790.
- (87) <http://www.mpip-mainz.mpg.de/documents/akbu/media/mech1.jpg>.

NOTE ADDED AFTER ASAP PUBLICATION

This paper was published on the Web on October 17, 2011. Due to a production error, several text revisions were added, and the corrected version was reposted on October 27, 2011.